

Filamentary current structures in the Madison Symmetric Torus

P. Piovesan^{1,2}, A. Almagri³, B.E. Chapman³, D. Craig³,
L. Marrelli¹, P. Martin^{1,2}, S.C. Prager³ and J.S. Sarff³

¹ Consorzio RFX, EURATOM-ENEA Association, Corso Stati Uniti 4, 35127 Padova, Italy

² Department of Physics, University of Padova, Italy

³ NSF Center for Magnetic Self-Organization in Laboratory and Astrophysical Plasmas and Department of Physics, University of Wisconsin, 1150 University Avenue, Madison, Wisconsin 53706, USA

Received 29 November 2007, accepted for publication 14 July 2008

Published 6 August 2008

Online at stacks.iop.org/NF/48/095003

Abstract

Filamentary structures are observed during edge relaxation events associated with spontaneous enhanced confinement periods in the Madison Symmetric Torus reversed-field pinch (Dexter R.N., Kerst D.W., Lovell T.W., Prager S.C. and Sprott J.C. 1991 *Fusion Technol.* **19** 131). The spatiotemporal shape of these structures is measured through extended toroidal and poloidal arrays of high-frequency magnetic probes at the plasma boundary. A simple model is used to interpret these structures as field-aligned current filaments, which are born at the reversal surface and propagate in the toroidal direction. The results found in MST share interesting commonalities with recent observations of filaments made during edge-localized modes in tokamaks and spherical tokamaks, as far as typical time scales, spatial localization and particle transport are concerned. Moreover, the dynamo effect produced by these events is estimated and compared with that produced during sawteeth. Though a single event has a small impact, the cumulative contribution of many of them produces a significant dynamo effect.

PACS numbers: 52.55.Hc, 52.55.Tn

(Some figures in this article are in colour only in the electronic version)

1. Introduction

Recent observations of edge-localized modes (ELMs) during H-mode in tokamaks and spherical tokamaks, made with a variety of diagnostics, such as arrays of magnetic probes, wide-angle cameras detecting visible light, thermography of wall structures, Thomson scattering, and others, have shed new light on their dynamics and spatiotemporal structure [1–6]. In particular these measurements have revealed that filamentary current structures aligned with the local magnetic field exist during ELMs. These have a direct impact on the way particles and energy are transported across the last closed flux surface and reach the wall and divertor target during these events. Modelling the nonlinear dynamics of these filaments may explain particle and energy losses during ELMs and thus allow one to predict their impact in future burning plasmas with greater confidence [7].

Small edge relaxation events sharing strong similarities with ELMs in tokamaks have been observed during enhanced confinement (EC) regimes in a reversed-field pinch (RFP) [8–11]. These events are usually associated with a burst of magnetic fluctuations in a broad range of frequency

[12]. This paper reports on the observation of filamentary current structures forming during these bursts, which are reminiscent of the filaments recently observed during ELMs. Measurements have been made in the Madison Symmetric Torus (MST) [13] RFP, based at the University of Wisconsin, Madison, WI, USA. The plasmas considered here are Ohmic discharges characterized by a spontaneous transition to EC, occurring under particular conditions described in [8–11]. The spatiotemporal shape of the individual bursts has been studied with extensive arrays of high-frequency magnetic probes, which densely cover the plasma along the toroidal and poloidal directions. Experimental evidence and modelling of the magnetic perturbation associated with these bursts indicate that each of them is associated with a field-aligned current filament originating near the edge. Information from various diagnostics demonstrates the impact of these structures on particle transport and dynamo.

Notwithstanding the significant impact of these structures on anomalous transport in the RFP, their nature is not yet clear. Various candidates may be proposed to explain them: drift-wave turbulence, current sheets generated by the nonlinear interaction of the dynamo modes, or pressure-driven g -modes.

Nonetheless, a definitive explanation still lacks. This paper aims to contribute to a better understanding of the bursts introduced above by providing a detailed characterization of their spatiotemporal structure and of their effects on particle transport and dynamo. Moreover, the similarities and differences with the ELM filaments in tokamaks are analysed.

The experimental apparatus, the diagnostics and the discharges analysed in this work are introduced in section 2. The spatiotemporal shape of the bursts is described in section 3, while section 4 illustrates a model that interprets them as field-aligned current filaments. The effects on particle transport and dynamo are discussed in sections 5 and 6, respectively. A discussion of their nature and a comparison with filament observations in tokamaks is proposed in section 7.

2. Experimental apparatus and discharge waveforms

RFPs are similar to tokamaks, but with a lower toroidal magnetic field, B_ϕ , whose amplitude is comparable to the poloidal field, B_θ , and reverses sign near the edge. As a consequence the RFP has a safety factor $q(r) = rB_\phi/(RB_\theta) \ll 1$ and is potentially unstable to a spectrum of tearing modes with poloidal and toroidal mode numbers $m = 1, n \gtrsim 2R/a$ and $m = 0, n \geq 1$. Here R and a are the torus major and minor radii, respectively. The $m = 1$ modes are internally resonant, while the $m = 0$ modes are localized to the reversal surface, where $B_\phi = 0$, which for typical RFP equilibria is placed at $r/a \approx 0.8$ – 0.9 . The standard RFP is sustained through a dynamo mechanism generated by the $m = 0, 1$ modes, hence the name dynamo modes, which are also responsible for anomalous transport through magnetic field stochasticization. Different types of operations with reduced magnetic chaos and consequent EC conditions are being investigated in the RFP community. Spontaneous transitions to EC are observed in MST under particular conditions: very clean wall, low density, relatively deep magnetic field reversal, $F = B_\phi(a)/\langle B_\phi \rangle$ ranging from -0.2 to -0.5 [8–11]. In these cases, a strong $\mathbf{E} \times \mathbf{B}$ sheared flow forms at the edge and the energy confinement time is roughly tripled. Sawtooth crashes become less frequent and smaller bursts dominated by the edge-resonant $m = 0$ modes appear between them, very likely destabilized by the strong pressure and/or current gradients forming at the edge [9, 11]. These smaller bursts have an intermittent character and are responsible for a large fraction of particle and thermal transport in the RFP [12].

The experiments described in the following were made in MST, a RFP with major radius $R = 1.5$ m and minor radius $a = 0.52$ m. A database of 60 similar deuterium discharges with spontaneous EC periods were analysed. All discharges have plasma current $I_p \simeq 0.6$ MA, electron density $n_e \simeq 1 \times 10^{19} \text{ m}^{-3}$, reversal parameter $F \simeq -0.2$, and pinch parameter $\Theta = B_\theta(a)/\langle B_\phi \rangle \simeq 1.8$.

The edge magnetic field fluctuations were measured with extensive arrays of pick-up coils along the poloidal and toroidal circumferences. For maximum sensitivity to small amplitude fluctuations, non integrated measurements of the toroidal magnetic field dB_ϕ/dt are taken. A schematic of the whole magnetic probe system is shown in figure 1: a toroidal array of

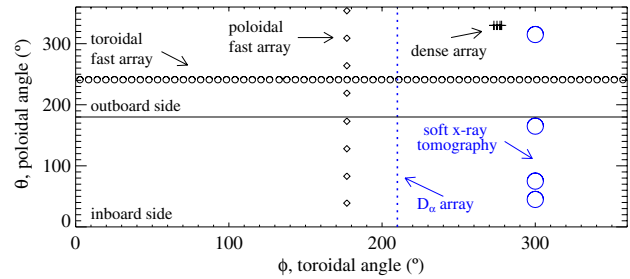


Figure 1. Schematic showing the toroidal and poloidal angles of the diagnostics used in this work.

64 equally spaced pick-up coils and a poloidal array of eight equally spaced pick-up coils measuring dB_ϕ/dt with 300 kHz frequency bandwidth; a toroidal array of 32 analog-integrated coils with frequency bandwidth $f < 100$ kHz, which is suitable for the detection of the $m = 0, 1$ dynamo modes; and a toroidally localized dense array of eight coils 1–2 cm apart with frequency bandwidth $f < 3$ MHz. Other diagnostics used in this work are a multichord soft-x-ray camera [14] and D_α detectors, which are also shown in figure 1.

The main waveforms of a typical EC discharge studied in this work are reported in figure 2. MST discharges are characterized by the cyclic occurrence of sawtooth crashes [15]. Their effect is visible in several plasma quantities. The core soft-x-ray brightness shows a slow phase of increase followed by a fast crash, with an outward propagating heat pulse. A burst of D_α emission following the sawtooth crash indicates the increased plasma–wall interaction taking place during this phase. This is a consequence of the increased thermal and particle transport caused by the destabilization of the $m = 0, 1$ dynamo modes at the sawtooth crash. They are also responsible for the regeneration of toroidal magnetic flux through dynamo action.

Periods far from major sawtooth crashes, which correspond to the spontaneous EC periods introduced above, are usually regarded as relatively quiescent, at least at low frequency, $f < 100$ kHz. However, it was shown that these periods are characterized by intermittent bursts of high-frequency, $f > 100$ kHz, magnetic fluctuations [8–11], as is also visible in the zoom of figure 2. We observe that these events have a small but clear effect on the soft-x-ray signal and the D_α emission. The internally resonant $m = 1$ modes are not significantly affected by the small bursts, while the $m = 0, n = 1, 2, 3$ modes instead are observed to transiently increase during them, as was shown for similar EC plasmas in [8–11]. Recent measurements with insertable probes showed that the $m = 0$ modes are linearly unstable during these periods [16]. A regeneration of the toroidal magnetic flux is associated with the small bursts, but much smaller than during sawteeth. These are the edge relaxation events introduced in the previous section and henceforth will be named *small bursts*.

3. Imaging of the small magnetic bursts

In this section we analyse the magnetic signals measured during the spontaneous EC discharges introduced above. Both the well-known major sawtooth crashes and the smaller bursts in between them are investigated. Figure 3 contains a contour

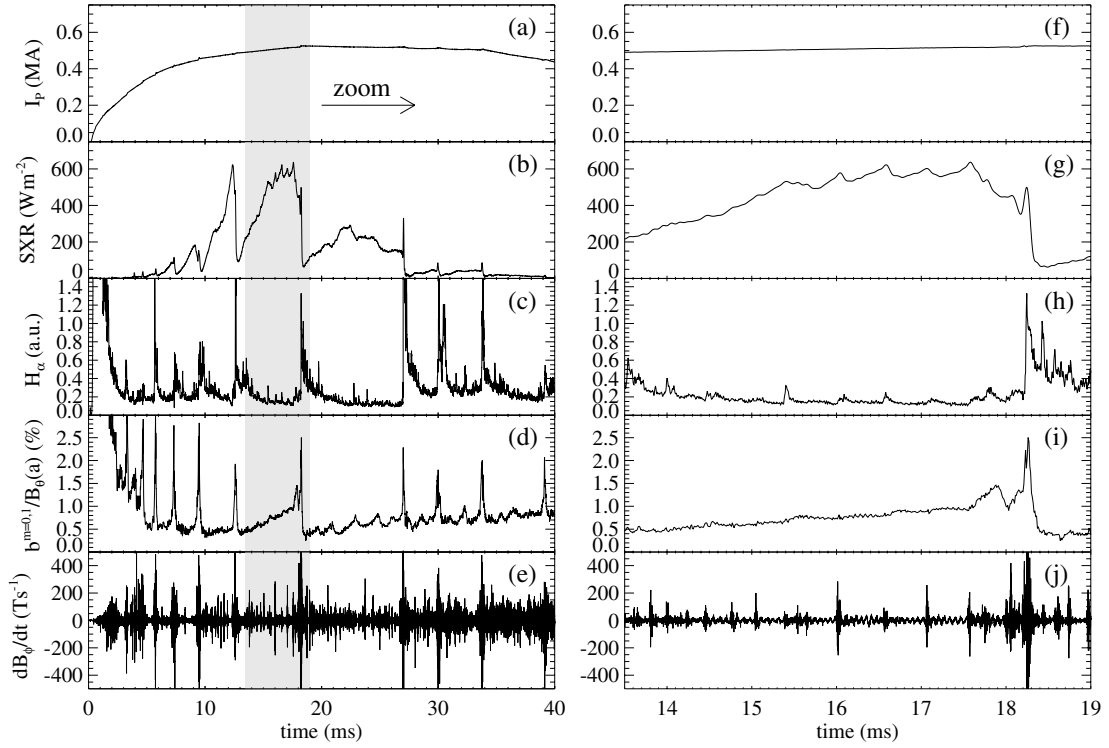


Figure 2. Waveforms of a typical EC discharge, 1051020091: (a), (f) plasma current, (b), (g) core soft-x-ray brightness, (c), (h) D_α emission, (d), (i) total relative amplitude of the $m = 0, 1$ modes, (e), (j) dB_ϕ/dt signal amplitude from a pick-up coil of the dense array high-pass filtered above 80 kHz. The zoom in the right column evidences the small bursts present in between sawteeth.

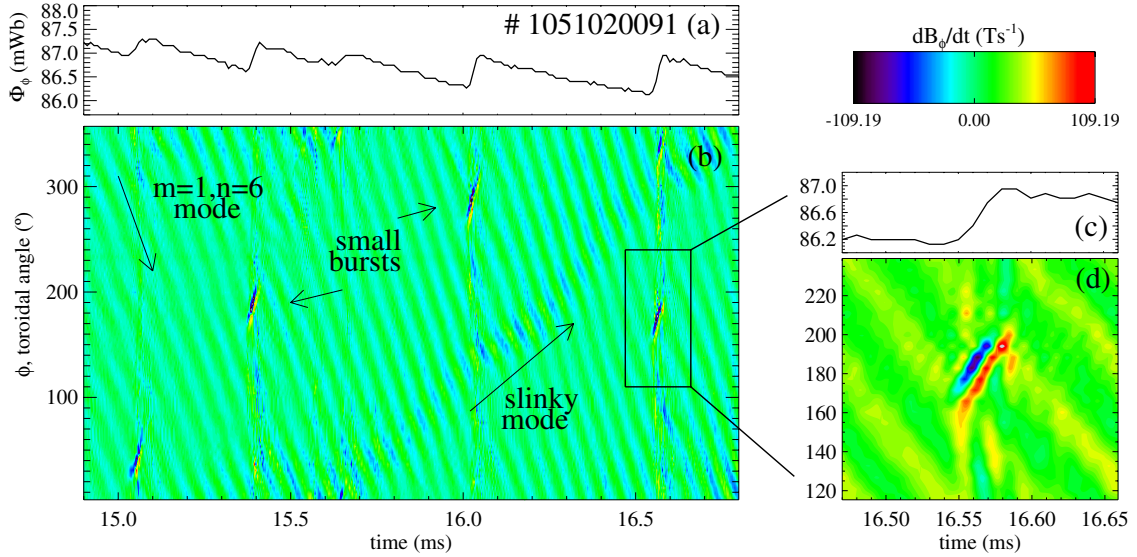


Figure 3. (a) Toroidal magnetic flux as a function of time for an EC discharge in a period between two sawtooth crashes. (b) Contour plot of the dB_ϕ/dt signal amplitude measured by the toroidal array of 64 pick-up coils as a function of toroidal angle and time. The arrows indicate the varied magnetic activity present in these periods and the zoom (c),(d) evidences the structure of a small burst.

plot of the dB_ϕ/dt signal amplitudes measured by the 64 probes of the toroidal array, as a function of toroidal angle and time during a period in between two sawtooth crashes. Here the crashes themselves are not included. The time evolution of the toroidal magnetic flux is also shown.

The arrows in figure 3 indicate the varied magnetic activity present during these relatively quiescent periods. We first note the $m = 1$ dynamo modes, and in particular the pattern of the

dominant $m = 1, n = 6$ mode, which rotates at a toroidal velocity $v_\phi \simeq 25 \text{ km s}^{-1}$. This is the innermost resonant $m = 1$ mode and typically dominates the magnetic spectrum in MST. We also observe the so-called *slinky* structure, which is a well-known toroidally localized perturbation formed by the nonlinear interaction of the $m = 0, 1$ modes [17].

We consider in figure 3 the small bursts introduced above. These are toroidally localized, appear at random toroidal

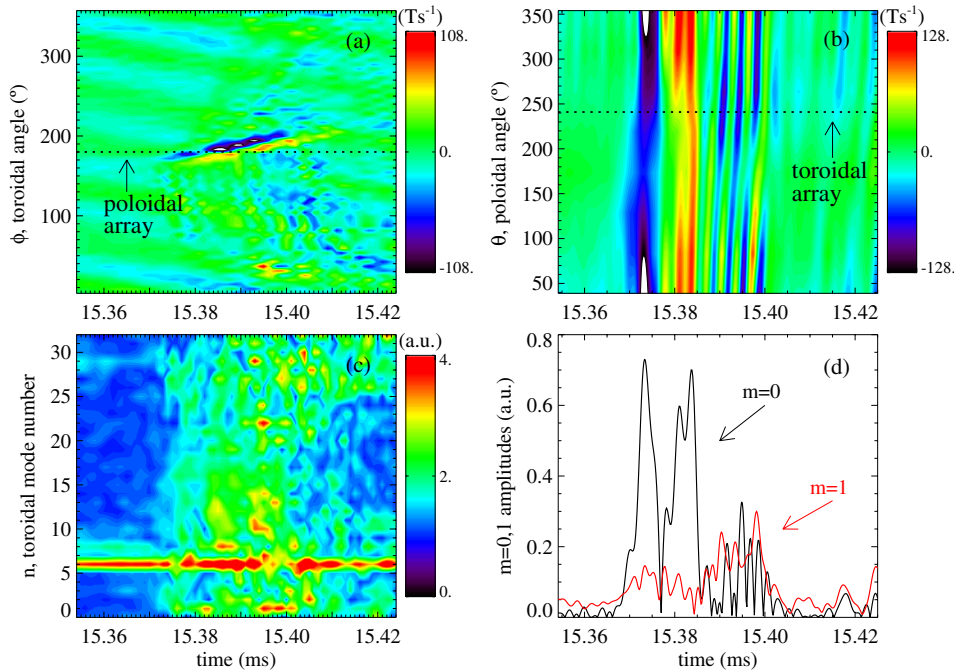


Figure 4. Contour plot of the dB_ϕ/dt signal amplitude measured during a small magnetic burst by (a) the toroidal and (b) poloidal arrays of pick-up coils as a function of time and angles. (c) Toroidal and (d) poloidal wave number amplitudes computed by Fourier decomposition of the measurements reported in (a) and (b), respectively.

angles and propagate in the direction opposite that of the internally resonant $m = 1$ modes, with a toroidal velocity in the range $25\text{--}55\text{ km s}^{-1}$, which is similar to the edge local flow velocity. These bursts are associated with a sharp increase in the toroidal magnetic flux, hence, as also shown in previous studies [8–11], they may be interpreted as small, discrete dynamo events. A zoom of a single burst is reported in figure 3 to show more clearly its spatiotemporal shape. The dB_ϕ/dt perturbation associated with the burst is formed by a maximum and a minimum propagating together in the toroidal direction. This implies that the respective B_ϕ perturbation is a toroidally localized propagating maximum. Such a structure is consistent with a field-aligned, i.e. mainly poloidal, current filament rotating in the toroidal direction, as will be better shown in the next section by means of a simple model.

The spatiotemporal shape of the small bursts has been determined by combining measurements from both the toroidal and the poloidal arrays of magnetic probes. Let us thus consider a burst observed simultaneously by the two arrays. Figures 4(a) and (b) show for such an event the dB_ϕ/dt signal amplitude measured by the toroidal and the poloidal arrays, respectively, as a function of angles and time. The toroidal and the poloidal mode number amplitudes computed by Fourier decomposition of these measurements are reported as a function of time in figures 4(c) and (d), respectively. We note here again in figure 4(a) the typical dB_ϕ/dt fluctuation pattern of the burst as a function of toroidal angle and time, with a minimum and a maximum propagating together in the toroidal direction, as already observed above. The frequency associated with this perturbation varies in the range $10\text{--}100\text{ kHz}$. Moreover, almost simultaneously with this dominant perturbation and also following it in this case, lower-amplitude perturbations are observed in figure 4(a), with a relatively high

$|n|$ ranging from 20 to 30, as can be deduced from figure 4(c), and higher propagation frequency varying in the range $120\text{--}300\text{ kHz}$.

A corresponding composite structure is also observed in figure 4(b) in the poloidal array. This shows in particular that the lower-frequency, toroidally localized perturbation has a dominant $m = 0$ shape. The higher-frequency fluctuations start growing simultaneously with this $m = 0$ perturbation and have a mixed $m = 0, 1$ harmonic content. By analysing the poloidal phase of the $m = 0, 1$ harmonics, it can be shown that they are coupled in a way to form a $m = 1$ perturbation with larger amplitude always at the outboard side: the $m = 0$ amplitude oscillates in time and is nonzero only when the maximum of the $m = 1$ perturbation is at the outboard side. These data are representative of all the bursts observed in the discharges analysed, as will be clear from the statistical analysis described below.

The average behaviour of an ensemble of 2622 events observed in 60 similar discharges has been studied to confirm the picture introduced above with a single example. Various physical quantities in this database, such as magnetic field perturbations, soft-x-ray and D_α brightness, have been averaged over a fixed time interval centred on the burst, to characterize the effect of the bursts on them. The time of the burst, t_0 , is chosen as the time when the toroidal magnetic flux starts to increase, while its toroidal angle, ϕ_0 , is the angle where the magnetic fluctuation of the burst is largest at $t = t_0$. Each quantity is then averaged over a time interval 0.2 ms long centred on t_0 . To analyse the toroidal shape of the perturbation in each quantity, the time average is conditioned to the angle where the burst occurs. This allows one to obtain the average perturbation to a particular quantity due to the burst as a function of time and toroidal angle. In particular we will be

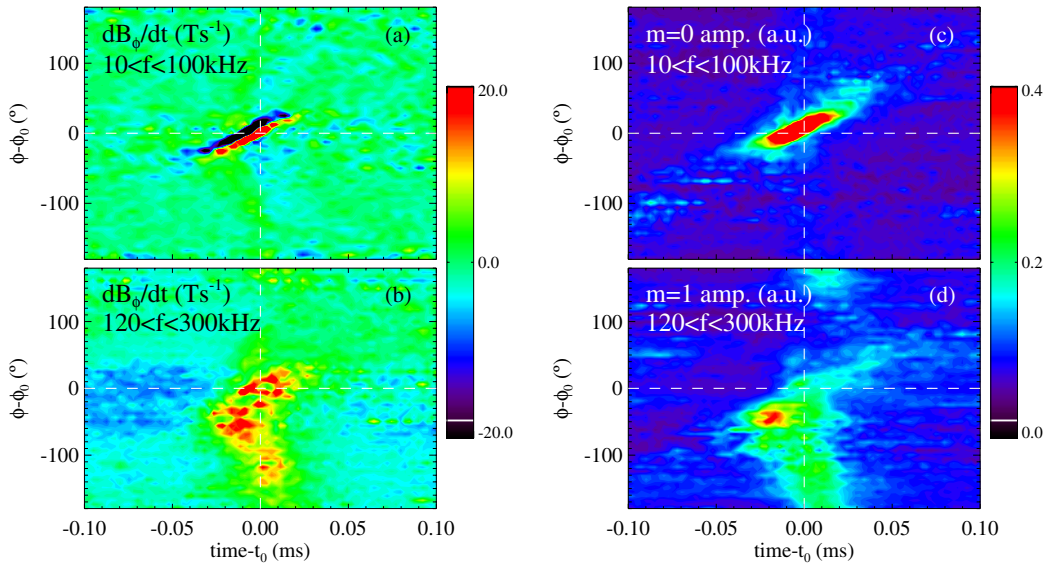


Figure 5. Ensemble-averaged perturbation due to the small bursts on different quantities as a function of toroidal angle and time: (a), (b) dB_ϕ/dt signal from a pick-up coil of the dense array in two frequency ranges; (c) $m = 0$ and (d) $m = 1$ amplitudes estimated from the poloidal array.

interested in checking if the perturbation to transport-related quantities is also toroidally localized.

To characterize the average spatiotemporal shape of the bursts and confirm the results observed on several single events, the conditional average analysis introduced above has been applied to magnetic signals measured at a fixed toroidal location. The signals analysed here are those from a probe of the dense array with 3 MHz bandwidth and those from the poloidal array with 300 kHz bandwidth. The faster probe was used to verify if fluctuations with $f > 300$ kHz, not detectable by the slower probes, were present during the bursts, which turned out not to be the case. To separate the contributions from the toroidally localized $m = 0$ perturbation and that from the $m = 1$ perturbation described in figure 4, the signals have been band-pass filtered in the respective frequency ranges identified before, 10–100 kHz and 120–300 kHz. Since the frequency ranges corresponding to the $m = 0$ and $m = 1$ perturbations are quite broad and in some case might slightly overlap, the intermediate frequency interval 100–120 kHz is not included in the analysis, to better separate contributions from these two types of perturbations. The results of this analysis are reported in figures 5(a) and (b), where it can be seen that the toroidal shape of the lower-frequency perturbation reproduces very well that of the $m = 0$ perturbation shown in figure 4(a), while the higher-frequency pattern closely resembles the behaviour of the $m = 1$ fluctuations in the same figure. The higher-frequency perturbations start simultaneously with the lower-frequency ones and propagate in both toroidal directions.

To confirm that the two types of perturbations described above have also the right poloidal dependence, the signals from the poloidal array have been ensemble averaged in a way similar to that described in the previous paragraph. They have first been band-pass filtered in the frequency ranges 10–100 kHz and 120–300 kHz and then Fourier decomposed to obtain the $m = 0$ and $m = 1$ amplitudes, respectively, as a function of time for each event. The amplitude signals obtained in this way for each burst are then ensemble averaged.

The average spatiotemporal distribution of the $m = 0, 1$ harmonics could be thus obtained and the results are shown in figures 5(c) and (d), respectively. The spatiotemporal pattern of the $m = 0, 1$ amplitudes resembles that obtained from a single probe. This shows that the two types of perturbations forming the burst have the same poloidal harmonic content identified in the single events.

This statistical analysis thus confirms the following picture for the small bursts. They are composed mainly of edge-resonant perturbations: a $m = 0$ toroidally localized perturbation grows simultaneously with $m = 1$ perturbations with relatively high $|n|$ of both signs, which correspond to helicities resonant very close to the reversal surface. Moreover, these edge perturbations seem not to interact strongly with the internally resonant $m = 1$ dynamo modes, which maintain their amplitude practically unchanged. A small effect on the $m = 0$ dynamo modes is instead observed, as was shown in several previous publications [8–11, 18, 19]. The relation between the localized $m = 0$ perturbation evidenced above and the $m = 0, n = 1, 2, 3$ modes is not yet clear and needs to be further investigated. A possible interpretation is that the toroidally localized $m = 0$ structures are the nonlinear evolution of the low-frequency $m = 0, n = 1, 2, 3, \dots$ modes. This has to be verified with simultaneous measurements of the $m = 0$, low n modes, which were not possible in the present experiments. In fact due to problems in the numerical integration of the dB_ϕ/dt signals, it was not possible with the present setup to measure simultaneously the small scale perturbations and the $m = 0$, low n component. Further experiments are needed to clarify this point.

Let us finally compare the spatial structure of the small bursts with that of a major sawtooth crash. A contour plot of the dB_ϕ/dt signal amplitude as a function of toroidal angle and time during a sawtooth crash is shown in figure 6. As would be expected, the magnetic perturbation associated with the sawtooth crash extends over the whole toroidal circumference. A large burst of the $m = 0, 1$ dynamo modes occurs during

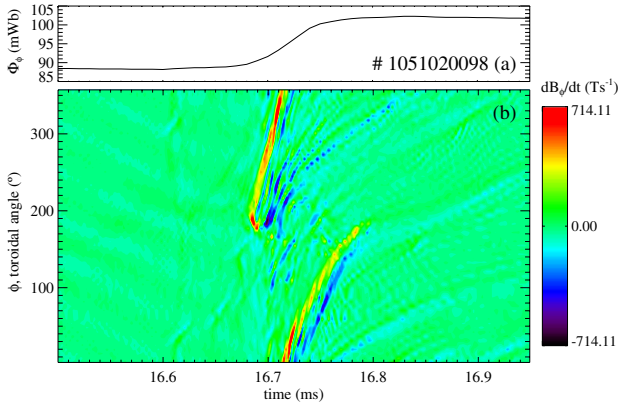


Figure 6. (a) Toroidal magnetic flux as a function of time during a sawtooth crash. (b) Contour plot of the dB_ϕ/dt signal amplitude measured by the toroidal array of 64 pick-up coils as a function of toroidal angle and time.

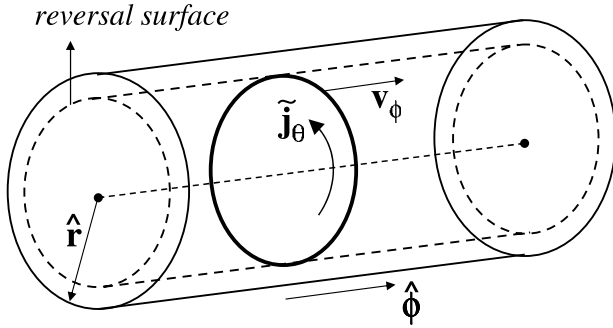


Figure 7. Schematic of the model current filament used to reproduce the magnetic fluctuations during the bursts. The filament is placed at the reversal surface, has $m = 0$ shape, and propagates in the toroidal direction.

the sawtooth crash, as already shown by several previous measurements [20]. It is interesting to note that the dominant $m = 0, n = 1$ component of the magnetic perturbation starts at a particular toroidal angle and then propagates around the entire torus. Similar results have recently been obtained also in the RFX-mod RFP machine, as described in [21].

4. The filament model

A simple model of a field-aligned current filament has been used to interpret the small bursts by fitting the perturbation to the dB_ϕ/dt signal produced by the moving filament and measured by the edge magnetic probes, and estimating the electric current flowing during a single burst. Such a picture is supported by previous measurements of the edge electric current made with an insertable Rogowski coil, which showed that the small $m = 0$ events correspond to an increase in the field-aligned current [22]. In addition the present results show that this current has a toroidally localized shape.

A schematic of the filament model in cylindrical geometry is shown in figure 7. A poloidal current filament with $m = 0$ shape is assumed to form during each burst at the reversal surface and rotate at a toroidal velocity v_ϕ . The reversal radius is estimated from reconstructions of the equilibrium magnetic field to be $r_{\text{rev}}/a \simeq 0.85$. The toroidal magnetic

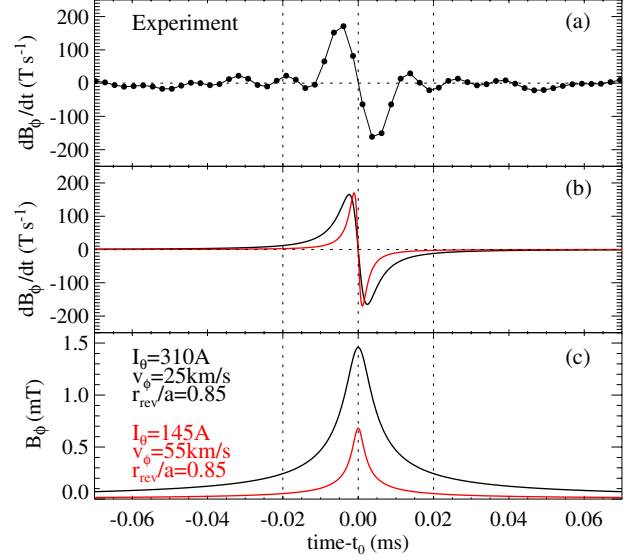


Figure 8. (a) dB_ϕ/dt perturbation at the toroidal angle of the small bursts $\phi = \phi_0$ averaged over the whole ensemble of events. (b) dB_ϕ/dt and (c) B_ϕ signals predicted by the filament model described in the text.

field perturbation produced by this moving current filament and sensed by a surface pick-up coil is computed from the following formula, assuming for simplicity that the filament can be approximated by a straight wire:

$$B_\phi(t) = \frac{\mu_0 I_\theta}{2\pi(\Delta^2 + v_\phi^2 t^2)^{1/2}}, \quad (1)$$

where $\Delta = a - r_{\text{rev}}$ is the distance between the reversal surface and the pick-up coil. In this simplified model the image current induced in the shell can be accounted for by multiplying by two the toroidal magnetic field measured by the pick-up coil. The only free parameter in this model is the electric current I_θ flowing in the filament, while the other parameters are fixed by measurements. This current has been varied in order to best fit the experimental data for two fixed values of the toroidal velocity $v_\phi = 25$ and 55 km s⁻¹, which correspond to the range of velocities observed over the ensemble of small bursts. Figure 8(a) reports the dB_ϕ/dt perturbation measured by edge pick-up coils as estimated from the ensemble average procedure described before. The model perturbation to the toroidal magnetic field and its time derivative due to the moving filament are reported in figures 8(b) and (c), respectively. By this fitting procedure, the current flowing in the filament is estimated to vary from $I_\theta \simeq 310$ A for $v_\phi = 25$ km s⁻¹ to $I_\theta \simeq 145$ A for $v_\phi = 55$ km s⁻¹.

Some mismatch between the experimental data and the model predictions is still present in figure 8. In particular, the experimental waveform is larger than the modelled ones, which might be attributed to the simplifications of the present model. In fact, the model does not take into account the finite spatial extent of the current filament, the time dependence of the amplitude and the fact that the filament is a loop and not a straight wire. A broadening of the temporal width in figure 8(a) could also be introduced by the ensemble average procedure, which combines together filaments with different toroidal velocities.

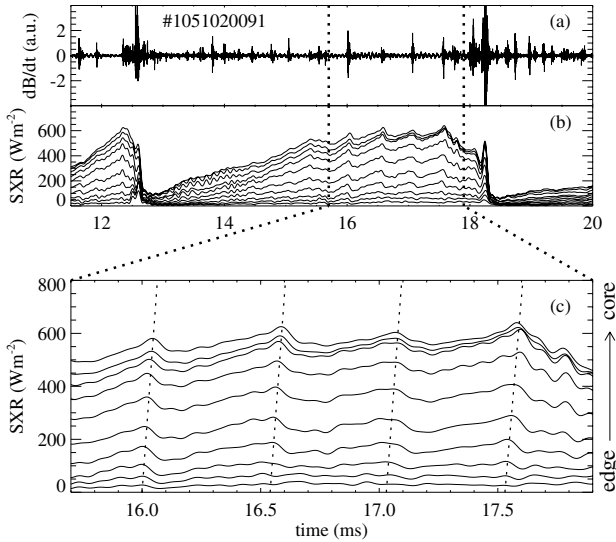


Figure 9. (a) Pick-up coil signal and (b), (c) soft-x-ray brightness signals from a fan of lines of sight spanning the plasma minor radius during an EC discharge. The zoom shows the inward propagating cold pulses due to the small magnetic bursts.

5. Effects of small bursts on soft-x-ray and D_α emission

The effect on transport-related quantities produced by both the major sawtooth crashes and the smaller bursts has been monitored with soft-x-ray and D_α detectors. Figure 9 reports the soft-x-ray brightness signals measured by a fan of lines of sight spanning the plasma minor radius. Two major sawtooth crashes occur here at $t = 12.5$ and 18.2 ms. The soft-x-ray brightness profile steadily increases in the period between sawteeth, reflecting the reduced thermal transport and the increase in the core electron temperature. An interesting phenomenon superimposed on these average dynamics is the smaller crashes evidenced in figure 9. These transiently interrupt the steady increase in the soft-x-ray emissivity and are triggered by the bursts studied above. Some magnetic bursts do not correspond to a soft-x-ray crash, probably because their amplitude is not large enough to produce a significant effect.

An interesting observation can be made by analysing the temporal delay of the soft-x-ray perturbations produced by the magnetic bursts along different lines of sight. In fact, as shown in figure 9, a cold pulse originating at the plasma edge propagates inwards to the core. Such an effect on the thermal profiles is very different from what is observed at the sawtooth crashes, where on the contrary an outward propagating heat pulse occurs. This is also compatible with the picture emerging from the fast magnetic measurements described above. In fact the small bursts mainly involve magnetic perturbations resonant near the reversal surface. Hence, it is very likely that the cold pulse is produced at the edge by these perturbations and then propagates to the core. A rough estimate of the electron heat diffusivity can be made by considering the radial distance travelled by the cold pulse $\Delta r \simeq 0.3$ m and the time taken $\Delta t \simeq 0.07$ ms. The perturbative heat diffusivity can be estimated as $\chi_e \simeq \Delta r^2 / \Delta t \simeq 1300 \text{ m}^2 \text{ s}^{-1}$. This is significantly larger than the typical power balance electron heat diffusivity in these plasmas amounting to about $200 \text{ m}^2 \text{ s}^{-1}$.

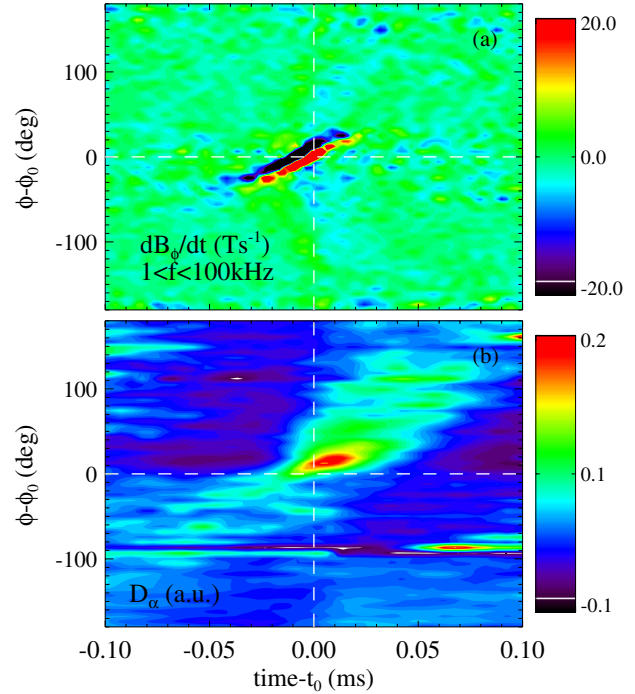


Figure 10. Ensemble-averaged perturbation due to the small magnetic bursts as a function of toroidal angle and time for (a) the dB_ϕ/dt signal amplitude from a pick-up coil of the dense array and (b) the D_α emission measured by an edge channel. The average is computed over the same ensemble of bursts as in figure 5.

This transient increase may be related to a larger turbulence level during the small bursts.

Since the small bursts have a toroidally localized shape, we may expect that their perturbation to quantities related to heat and particle transport has a similar localization. This is shown by computing the ensemble-averaged perturbation of the D_α signal as a function of time and toroidal angle, in a way similar to what was described in the previous section. The result is reported in figure 10(b), where we observe that the increase in D_α emission following the burst is localized to the toroidal position where the $m = 0$ filament occurs. This hints that the effect of the bursts may be that of locally enhancing the radial particle transport. In turn this may increase the plasma-wall interaction and cause a localized cold pulse. A similar localization could not be observed in the soft-x-ray emissivity from the edge region, which is perturbed in the same way at all toroidal angles. This may reflect the fact that these small bursts are composed of a toroidally localized filament, but also by longer-wavelength $m = 0, n = 1, 2, \dots$ modes. This last component may be responsible for the global effect observed on the soft-x-ray measurements.

The mechanism responsible for the enhanced, toroidally localized particle transport during the small bursts is not yet known, but some speculations can be made. One possibility is that the increased level of fluctuations transiently produces magnetic chaos. Nonetheless losses of a convective origin cannot be excluded at the moment based on the available experimental evidence. Future work will aim at better discriminating between the different possible loss mechanisms.

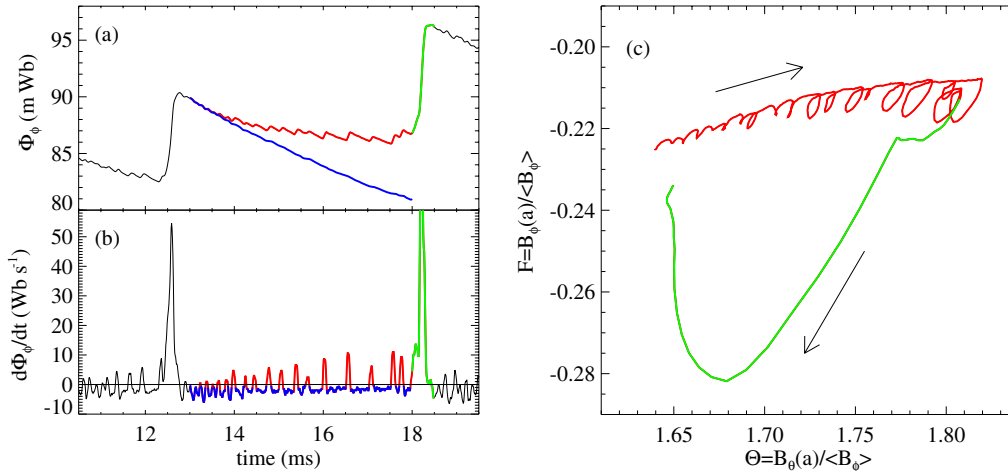


Figure 11. (a) Toroidal magnetic flux waveform and (b) its time derivative, showing the effect of two sawtooth crashes and of the small bursts in between them. The time evolution of the toroidal flux as computed in the absence of the small bursts is also added. (c) F - Θ curve during the same period.

6. Effects of small bursts on dynamo

It is well known that a continuous dynamo driven by slowly evolving $m = 0, 1$ modes exists in between sawteeth, though at a much lower level than during the main sawtooth crashes [20]. We show here that during EC periods the small bursts may also produce significant dynamo. This is evident in figure 11(a), where the toroidal magnetic flux is plotted as a function of time for a period in between two sawteeth, which occur with a large toroidal flux regeneration at $t \simeq 12.5$ and 18 ms. As observed also in figure 3, toroidal flux regeneration events occur in correspondence with the small bursts. The toroidal flux in these events increases by about 1%, which is quite small if compared with the 10% increase occurring during sawteeth. Nonetheless the total effect of several such bursts can be significant.

The cumulative dynamo effect of several small bursts in a period between sawteeth has been estimated by computing the time evolution of the toroidal magnetic flux in their absence. Figure 11(b) shows that the time derivative of the toroidal magnetic flux is quite constant during this period, apart from the jumps associated with the bursts. The time evolution of the toroidal magnetic flux has been computed based on its time derivative after having removed from it the jumps due to the bursts, where the derivative has positive values, and by replacing these values with a linear fit of the adjacent points. The result is shown with a blue line in figure 11(a), where it can be seen that the decrease in toroidal flux in the absence of the bursts would be significantly larger. The discrepancy among the measured and simulated flux just before the sawtooth crash amounts to about $\Delta\Phi \simeq 5$ mWb, which is comparable to the contribution of the sawtooth crash. The same calculation has been made for all the discharges in the database and the results confirm on average the above evidence. Figure 11(c) shows the dynamics of the F - Θ curve for sawteeth and small bursts. It is interesting to note that the circular patterns associated with the small bursts are analogous to that produced by the sawtooth crash, confirming once again the similar dynamo effect on the magnetic field profiles.

The cumulative effect of several bursts may thus significantly contribute to the dynamo in EC periods. A

questionable point is whether all the dynamo is produced by the $m = 0$ filament, which seems quite unreasonable given its high localization and total current flowing in it, or if the $m = 0$ dynamo modes also play a role. Internally resonant $m = 1$ modes seem not to vary during small crashes, but the $m = 0, n = 1, 2, 3$ modes become unstable during the bursts, as observed in [16].

7. Summary and discussion

Measurements of the spatiotemporal shape of magnetic bursts occurring during spontaneous EC periods in MST have been reported. Extensive arrays of fast magnetic probes have been used to obtain a detailed picture of these events. These exhibit a composite magnetic structure: they are dominated by a toroidally localized perturbation with $m = 0$ shape, which has been interpreted as a field-aligned current filament; a broad spectrum of $m = 1$, high- n fluctuations, originating at the toroidal angle where the filament is born, are destabilized simultaneously with the $m = 0$ filament and propagate in both toroidal directions. It is not yet clear if the filament destabilizes the higher-frequency fluctuations or if it is triggered by them.

Individually, the small bursts have a small impact on transport and dynamo, but their cumulative effect may provide an important contribution in between sawteeth. A quantitative estimate of the transport and dynamo produced by the bursts would require measurements of the edge radial profiles with high spatiotemporal resolution. In particular, it would be interesting to compare the relative contribution of the toroidally localized filament and of the long-wavelength dynamo modes associated with the bursts.

Important information on the small bursts studied so far was recently provided by measurements made with insertable magnetic and Langmuir probes in 0.2 MA EC plasmas [16]. The linear and nonlinear drive of the $m = 0$ modes could be measured both during standard sawteeth and small bursts. During sawteeth the $m = 0$ modes are shown to be driven by the nonlinear coupling of a broad spectrum of $m = 1$ modes, while they are linearly unstable during the small bursts. The $m = 0$ modes are likely driven by the strong edge pressure

and/or current gradients forming during EC periods. It is important to stress that the results discussed in [16] refer to the $m = 0$, $n = 1, 2, 3$ modes. The high- n , toroidally localized component described in this work was not identified in the earlier studies with insertable probes, which are not suited to measurements in the high plasma current discharges analysed here. Unfortunately, as explained above, measurements of the long-wavelength $m = 0$ perturbation were not possible in the present experiments. Nonetheless a link among such different scales may be present and is certainly worth investigating in the future.

Clear evidence of edge bursts such as those studied in this paper has not yet been found in nonlinear MHD simulations of the RFP, such as those made with the DEBS [23] and SpeCyl [24] codes. This may be due to the fact that finite pressure effects are not included in a self-consistent way in these codes. Interestingly recent nonlinear simulations of pulsed parallel current drive (PPCD) plasmas made with DEBSP, a version of DEBS including pressure, show that the $m = 0$ modes are not efficiently stabilized by PPCD and continue to have a finite amplitude, probably due to the strong edge pressure gradient associated with EC conditions [25, 26]. These results suggest that pressure driven modes may play a significant role in EC plasmas. Hopefully a dedicated numerical study may explain the experimental results described in this paper.

Several interesting parallels exist among the results of this work and analogous observations of filamentary structures made in tokamaks and spherical tokamaks. First of all both in RFP and tokamaks the filaments are associated with a field-aligned current perturbation that rotates in the toroidal direction with velocities comparable to the local fluid velocity. Currents of about 100–200 A are estimated to flow through each filament in MAST [1] with a simple current wire model similar to that used here and similar filament currents of about 150–300 A are measured in MST. Nonetheless it must be stressed that the ELM filaments in tokamaks cannot be regarded as closed current-carrying loops, as in the present model, since they intersect the divertor. Another similarity regards the typical lifetime of the filaments, which is of 50–100 μs in MST and of about 100–200 μs in MAST and other tokamak experiments [1–6].

Also the transport effects of these filamentary structures have some similarities. In particular D_α measurements show that the filament produces a toroidally localized perturbation to the particle transport, which is quite similar to the tokamak case. Nonetheless while in tokamaks the energy and particle losses occur mainly along the filament, in the RFP the transport mainly occurs in the direction perpendicular to it. Moreover, the radial position of the filaments is different. In the RFP the filaments are born at the reversal surface, while in tokamaks they originate near the pedestal region. Information on the radial movement of the filament is lacking at present in MST and may be the subject of future studies. Nonetheless, since the filaments maintain a clear $m = 0$ structure during their existence, which suggests that they are born and exist near the reversal surface, it may be speculated that their radial position does not vary significantly in time.

A significant difference among RFP and tokamak observations regards the number of filaments observed during a

single event. These are of the order of 10–20 in most tokamak cases during Type I ELMs, while only one or at most two filaments are observed in the RFP at a time. Nonetheless it should be mentioned that a case exists in which single or double filaments are observed in spherical tokamaks. This happens during Type V ELMs in NSTX [3]. At the moment a definitive explanation of this phenomenon is lacking in both cases, but the similarity of these results suggests that interesting common physics may exist.

One more parallel regards a possible model of these filaments in RFPs and recent theoretical developments in tokamaks. A nonlinear peeling–ballooning model seems to be the best candidate for explaining these structures in tokamaks [27]. The peeling mode stability has recently been described in terms of a Taylor relaxation of an edge annulus of plasma current [28]. Such a description has interesting similarities with theories that describe the RFP relaxation and thus may be extended to explain the bursts studied in this work. Nonetheless, the nature of the perturbations involved in these events may be different in the two configurations. Tearing modes driven by edge and/or pressure gradients are the most probable candidates in the RFP, while coupled peeling–ballooning modes dominate the ELM dynamics in tokamaks.

Acknowledgments

Three of the authors (P.P., L.M., P.M.) would like to thank the whole MST team for the continuous and strong support during the experimental activity. We also acknowledge useful discussions with D.F. Escande and E. Martines. This work was supported by the European Communities under the contract of Association between EURATOM/ENEA. The views and opinions expressed herein do not necessarily reflect those of the European Commission.

References

- [1] Kirk A. *et al* 2005 *Plasma Phys. Control. Fusion* **47** 995
- [2] Kirk A. *et al* 2006 *Plasma Phys. Control. Fusion* **48** B433
- [3] Maingi R. *et al* 2006 *Phys. Plasmas* **13** 092510
- [4] Leonard A.W. *et al* 2006 *Plasma Phys. Control. Fusion* **48** A149
- [5] Schmid A., Herrmann A., Müller H.W. and the ASDEX Upgrade Team 2008 *Plasma Phys. Control. Fusion* **50** 045007
- [6] Neuhauser J. *et al* 2008 *Nucl. Fusion* **48** 045005
- [7] Wilson H.R., Cowley S.C., Kirk A. and Snyder P.B. 2006 *Plasma Phys. Control. Fusion* **48** A71
- [8] Chapman B.E., Almagri A.F., Cekic M., Den Hartog D.J., Prager S.C. and Sarff J.S. 1996 *Phys. Plasmas* **3** 709
- [9] Chapman B.E., Chiang C.-S., Prager S.C., Sarff J.S. and Stoneking M.R. 1998 *Phys. Rev. Lett.* **80** 2137
- [10] Chapman B.E. *et al* 1998 *Phys. Plasmas* **5** 1848
- [11] Chapman B.E. 1997 Fluctuation reduction and enhanced confinement in the MST reversed field pinch *PhD Thesis* University of Wisconsin, Madison, WI
- [12] Marrelli L., Frassinetti L., Martin P., Craig D. and Sarff J.S. 2005 *Phys. Plasmas* **12** 030701
- [13] Dexter R.N., Kerst D.W., Lovell T.W., Prager S.C. and Sprott J.C. 1991 *Fusion Technol.* **19** 131
- [14] Franz P., Bonomo F., Gadani G., Marrelli L., Martin P., Piovesan P., Spizzo G., Chapman B.E. and Reyfman M. 2004 *Rev. Sci. Instrum.* **75** 4013
- [15] Hokin S. *et al* 1991 *Phys. Fluids B* **3** 2241

- [16] Choi S., Craig D., Ebrahimi F. and Prager S.C. 2006 *Phys. Rev. Lett.* **96** 145004
- [17] Almagri A.F., Assadi S., Prager S.C., Sarff J.S. and Kerst D.W. 1992 *Phys. Fluids B* **4** 4080
- [18] Chapman B.E. *et al* 2001 *Phys. Rev. Lett.* **87** 205001
- [19] Chapman B.E. *et al* 2002 *Phys. Plasmas* **9** 2061
- [20] Den Hartog D.J., Chapman J.T., Craig D., Fiksel G., Fontana P.W., Prager S.C. and Sarff J.S. 1999 *Phys. Plasmas* **6** 1813
- [21] Zuin M. *et al* 2008 Current sheets driven by spontaneous reconnection in a current-carrying fusion plasma to be submitted
- [22] Chapman B.E. *et al* 2000 *Phys. Plasmas* **7** 3491
- [23] Schnack D.D., Barnes D.C., Mikic Z., Harned D.S. and Caramana E.J. 1987 *J. Comput. Phys.* **70** 330
- [24] Cappello S. and Biskamp D. 1996 *Nucl. Fusion* **36** 571
- [25] Dahlin J.-E. and Sheffel J. 2007 *Nucl. Fusion* **47** 9
- [26] Dahlin J.-E., Sheffel J. and Anderson J.K. 2007 *Plasma Phys. Control. Fusion* **49** 183
- [27] Wilson H.R. and Cowley S.C. 2004 *Phys. Rev. Lett.* **92** 175006
- [28] Gimblett C.G., Hastie R.J. and Helander P. 2006 *Phys. Rev. Lett.* **96** 035006